On the nature of the mHz X-ray QPOs from ULX M82 X-1: Evidence for Timing-Spectral (anti) correlation

Dheeraj R. Pasham[1] & Tod E. Strohmayer[2]

ABSTRACT

Using all the archival *XMM-Newton* X-ray (3-10 keV) observations of the ultraluminous X-ray source (ULX) M82 X-1 we searched for a correlation between its variable mHz quasi-periodic oscillation (QPO) frequency and its energy spectral power-law index. These quantities are known to correlate in stellar mass black holes (StMBHs) exhibiting Type-C QPOs (∼0.2-15 Hz). The detection of such a correlation would strengthen the identification of its mHz QPOs as Type-C and enable a more reliable mass estimate by scaling its QPO frequencies to those of Type-C QPOs in StMBHs of known mass. We resolved the count rates of M82 X-1 and a nearby bright ULX (source 5/X42.3+59) through surface brightness modeling and identify observations in which M82 X-1 was at least as bright as source 5. Using only those observations, we detect QPOs in the frequency range of 36-210 mHz during which the energy spectral power-law index varied from 1.7-2.2. Interestingly, we find evidence for an anti-correlation (Pearson's correlation coefficient = -0.95) between the power-law index and the QPO centroid frequency. While such an anti-correlation is observed in StMBHs at high Type-C QPO frequencies (∼5-15 Hz), the frequency range over which it holds in StMBHs is significantly smaller (factor of $\sim$ 1.5-3) than the QPO range reported here from M82 X-1 (factor of 6). However, it remains possible that contamination from source 5 can bias our result. Joint *Chandra/XMM-Newton* observations in the future can resolve this problem and confirm the timing-spectral anti-correlation reported here.

Subject headings: X-rays: binaries: Accretion disks: Methods: Data analysis

---

[1]Astronomy Department, University of Maryland, College Park, MD 20742; dheeraj@astro.umd.edu

[2]Astrophysics Science Division, NASA's Goddard Space Flight Center, Greenbelt, MD 20771; email: tod.strohmayer@nasa.gov

1. Introduction

The bright, point-like, non-nuclear X-ray sources in nearby galaxies with X-ray (0.3-10.0 keV) luminosities in the range of a few$\times 10^{39-41}$ ergs s^{-1} are known as the Ultra-Luminous X-ray sources (ULXs). Their variability on short timescales (some ULXs are known to vary on timescales of the order of a few minutes) combined with high X-ray luminosities suggests that these sources are powered by accretion of matter onto black holes (excluding the X-ray bright supernovae: e.g., Immler & Lewin 2003). But the masses of these black holes is still controversial. The current arguments suggest that ULXs are either powered by stellar-mass black holes (StMBH: mass range of 3-50 $M_{\odot}$) accreting matter via a super-Eddington mechanism (e.g., Körding et al. 2002; King et al. 2001; Begelman 2002; Gladstone et al. 2009), or that they comprise Intermediate-Mass Black Holes (IMBHs: mass range of a few$\times$(100-100) $M_{\odot}$) accreting at a sub-Eddington rate (Colbert & Mushotzky 1999). There is, however, no clear consensus on either scenario.

A subsample of ULXs show X-ray quasi-periodic oscillations (QPOs). These include NGC 5408 X-1 (centroid frequencies of $\approx$ 10-40 mHz: Strohmayer et al. 2007; Strohmayer & Mushtozky 2009; Dheeraj & Strohmayer 2012), NGC 6946 X-1 (centroid frequency of 8.5 mHz: Rao et al. 2010), M82 X-1 (centroid frequencies of $\approx$ 50-170 mHz: Strohmayer & Mushtozky 2003; Dewangan et al. 2006; Mucciarelli et al. 2006) and X42.3+59 (centroid frequencies of 3-4 mHz: Feng et al. 2010). In particular, the qualitative nature of the power density spectra (PDS) of NGC 5408 X-1, NGC 6946 X-1 and M82 X-1 is similar and can be described by a flat-topped, band-limited noise breaking to a power-law with QPOs evident on the power-law portion of the PDS, close to the break. This is strikingly similar to the PDS of StMBHs, when they exhibit the so-called "type-C" Low-Frequency QPOs (LFQPOs: frequency range of $\approx$ 0.2-15 Hz). However, the crucial difference is that the characteristic frequencies within the PDS of the ULXs, viz., the break frequency and the centroid frequency of the QPOs are scaled down by a factor of approximately 10-100 compared to the StMBHs with type-C LFQPOs. It has thus been argued that the mHz QPOs (10-200 mHz) of ULXs are analogs of the type-C LFQPOs of StMBHs and that the observed difference in the characteristic frequencies (a few$\times$(0.01-0.1) Hz compared with a few Hz) is due to the presence of massive black holes ($>$ mass of the StMBHs) within the ULX systems.

Furthermore, it has been established recently (e.g., McHardy et al. 2006; Körding et al. 2007) that the break frequency of the PDS of StMBHs and super-massive black holes scales inversely with the mass of the black hole (after accounting for the differences in the accretion rates, i.e., luminosities of the sources). In addition, it is known that the centroid frequency of the LFQPOs of StMBHs scales directly with the break frequency of the PDS (Wijnands

& van der Klis 1999; Klein-Wolt & van der Klis 2008). Therefore, it is reasonable to assume that the centroid frequency of the type-C LFQPOs and its analogs, if any, in ULXs & AGN should scale with the mass of the host black hole. This is complicated by the fact that the LFQPOs in StMBHs are variable and occur in a wide range of frequencies ($\approx$ 0.2-15 Hz). But, combining spectral information has proven to be useful. One of the distinctive features of the type-C LFQPOs of StMBHs is that their variable centroid frequency is strongly correlated with the index of the power-law component of the energy spectrum. The trend can be described as an increase in the power-law index with increase in the centroid frequency of the QPO with an evidence for turn-over, i.e., decrease of the power-law index with increase in the QPO centroid frequency, beyond a certain high QPO frequency (see Figure 10 of Vignarca et al. 2003). Therefore, at a given value of the energy spectral power-law index, the QPO frequency scales directly with the mass of the black hole. Hence, under the assumption that a mHz QPO from a certain ULX is an analog of the type-C LFQPO of StMBHs, the mass of its black hole can be estimated by measuring the QPO frequency from the PDS and the power-law index from its energy spectrum.

This technique of estimating black hole masses of ULXs has been implemented by various authors. For example, Dewangan et al. (2006) extracted the PDS and the energy spectrum of M82 X-1 and found the QPO centroid frequency and the power-law index of the energy spectrum to be $\approx$ 114 mHz and $\approx$ 2.0, respectively. Using the QPO frequency - photon index correlation of two StMBH sources, GRS 1915+105 and XTE J1550-565, as a reference they estimated the mass of the black hole in M82 X-1 by scaling its QPO frequency (114 mHz) at the given photon index (2.0). They estimated the mass to be in the range of 25-500 $M_{\odot}$ (see also, Mucciarelli et al. 2006). Similar scaling arguments were used by Rao et al. (2010) to estimate the mass of the black hole in the ULX NGC 6946 X-1 to be in the range (1-4)$\times$1000 $M_{\odot}$. Based on both the PDS and the X-ray energy spectrum of NGC 5408 X-1, Strohmayer & Mushotzky (2009) argued that the source behavior was consistent with the steep-powerlaw state (SPL) often seen in StMBHs. They compared the available data from NGC 5408 X-1 to five different StMBH reference sources and estimated the mass of the black hole to be $\sim$ a few$\times$1000 $M_{\odot}$.

It is crucial to realize that all the current black hole mass estimates of ULXs, that rely on scaling QPO frequencies at a given power-law index, assume that the mHz QPOs seen in ULXs are the analogs of the type-C LFQPOs of StMBHs. In this article, we test this hypothesis in the case of ULX M82 X-1, by investigating if the QPOs detected from ULX M82 X-1 show the same characteristic behavior of type-C LFQPOs of StMBHs, i.e., *whether M82 X-1's QPO frequency is correlated with the power-law index of its energy spectrum.* Similar attempts have been made earlier by Fiorito & Titarchuk (2004) for the case of M82 X-1 and more recently by Dheeraj & Strohmayer (2012) for the case of NGC 5408 X-1. The

work by Fiorito & Titarchuk (2004) considered only one *XMM-Newton* observation and three *RXTE/PCA* observations and was severely limited by the observed variability of M82 X-1's QPO frequencies, i.e, 50-100 mHz. In addition, they did not consider the contamination by a nearby bright X-ray source (source 5/X42.3+59) in their spectral modeling. Here we include analysis using all of the archival *XMM-Newton* observations that show QPOs from the range of 36 mHz (the lowest ever reported from M82 X-1) to 210 mHz (the highest QPO frequency reported from M82 X-1).

This article is arranged as follows. In Section 2, we describe all of the *XMM-Newton* observations used in the present study and carry out surface brightness modeling of their MOS1 images. In Section 3, we show results from our timing and spectral analysis where we model the PDS and the energy spectra of all the observations used in this study. We also show the two primary results of this article: (1) evidence for an anti-correlation between the centroid frequency of the QPO and the power-law index of the energy spectra and (2) the correlation between the average count rate and the centroid frequency of the QPO. In Section 4, we compare these results with StMBHs with type-C QPOs. We discuss the implications of the observed correlations on the mass of the black hole within M82 X-1. We also address the various caveats concerning the observed anti-correlation.

2. *XMM-Newton* observations and surface brightness modeling

Prior to the present work, QPOs have been reported from M82 X-1 using the *RXTE/PCA* (Strohmayer & Mushotzky 2003; Kaaret et al. 2006; Mucciarelli et al. 2006) and the *XMM-Newton*/EPIC data (Mucciarelli et al. 2006; Dewangan et al. 2006). *RXTE*'s PCA is a non-imaging detector whose field of view includes various point sources nearby M82 X-1. Its data does not allow one to disentangle the contribution from the nearby bright sources. However, data acquired with *XMM-Newton* allows for surface brightness modeling that can help us understand M82 X-1's relative brightness with respect to nearby sources. Also, *XMM-Newton* observations have longer exposures which allow high-quality energy spectra and firm detection of the QPOs. Due to these reasons, we decided to use only the data obtained from *XMM-Newton*. To date, *XMM-Newton* has observed M82 on twelve occasions. Three of these observations were severely effected by flaring. We analyzed the remaining nine observations to search for the presence of QPOs. We detected QPOs in six of them. Since the present work relies on searching for correlation between the QPO frequency and the energy spectral power-law index, we only considered the observations with QPOs. The *XMM-Newton* assigned IDs of the six observations used in this article are 0112290201, 0206080101, 0657800101, 0657801901, 0657802101 and 0657802301. The total observing times are 30 ks,

104 ks, 26 ks, 28 ks, 22 ks and 23 ks, respectively.

At *XMM-Newton*'s spatial resolution the flux from M82 X-1 is contaminated by the diffuse X-ray emission from the host galaxy (e.g., Strickland & Heckman 2007) and the nearby point sources (Matsumoto et al. 2001). Careful X-ray spectral modeling by various authors including Mucciarelli et al. (2006) and Caballero-García (2011) has shown that the diffuse component is dominant at energies below 3 keV. Therefore, to eliminate its contribution, we only included events in the energy range of 3.0-10.0 keV. Similar exclusions have been employed by Strohmayer & Mushotzky (2003) and Fiorito & Titarchuk (2004). The observations taken by the high-resolution camera onboard *Chandra* have revealed that there are a total of nine point sources within the 10"×10" region around M82 X-1 (Matsumoto et al. 2001). In principle, the flux contribution from these point sources can bias the spectral modeling of M82 X-1. Chiang & Kong (2011) have analyzed all of the archival *Chandra* observations of M82 to study the long-term (1999-2007) variability of the X-ray point sources within M82. They find that while the X-ray sources nearby M82 X-1 are variable, the maximum observed X-ray (0.3-8.0 keV) luminosity of these sources is $\lesssim 1/5^{th}$ the average luminosity of M82 X-1 (see Table 2 of Chiang & Kong 2011). Hence, they may not severely effect the spectral modeling of M82 X-1. However, source 5 (as defined in Matsumoto et al. 2001) is an exception. It can reach X-ray luminosities comparable to M82 X-1 (Feng & Kaaret 2007). Therefore, to estimate the amount of contamination by source 5 in each of the observations, we carried out surface brightness modeling of the images assuming they are dominated by two point sources.

We used only the MOS1 data for the purposes of surface brightness modeling. This is due to the fact that the MOS data offers the finest pixel size of 1.1" compared to the 4.1" of the EPIC-pn. Furthermore, the image resolution of EPIC-pn is close to the separation (≈ 5") between source 5 and M82 X-1 (Feng & Kaaret 2007). We avoid MOS2 data because its point spread function (PSF) is non-axisymmetric at the core. The on-axis PSF of MOS1 can be adequately described by an axisymmetric 2D king model (*XMM-Newton* current calibration file release notes 167). Similar to the analysis of Feng & Kaaret (2007) (who also carried out surface brightness modeling of *XMM-Newton*'s MOS1 data from M82 using a king model), we used the *calview* tool with an EXTENDED accuracy level to extract an on-axis PSF at an energy of 3.0 keV. We then fit a king model[1] to this PSF. The best-fit values of the core

[1]

$$PSF_{king} = \frac{N}{\left[1 + \left(\frac{r}{r_0}\right)^2\right]^{\alpha}}$$

where r_0, α and N are the core radius, index and the normalization, respectively.

radius and the index are 4.0" and 1.39, respectively. We note that these values are consistent with the best-fit parameters given in the latest calibration file XRT1_XPSF_0014.CCF and also with the values reported in the MOS calibration documentation (*XMM-Newton* current calibration file release notes 167).

From each of the six *XMM-Newton* observations, we extracted a MOS1 image of size 21"×21" binned to 1"×1" (square pixels) and roughly centered on M82 X-1. The standard filters of *FLAG==0* and *PATTERN<=12* were applied. As mentioned earlier, all the images were extracted in the energy range of 3.0-10.0 keV to reduce the influence of the diffuse X-ray emission from the host galaxy. Each of these MOS1 images were then modeled with two PSFs to represent source 5 and M82 X-1. The core radius and the spectral index of the two PSFs were fixed at the best-fit values, i.e., 4.0" and 1.39, respectively. The centroids (x, y) and the normalizations of the two PSFs were allowed to vary. However, the distance between the two sources was fixed to the values found using the co-ordinates reported by Feng & Kaaret (2007). We ignore the background as it was negligible in all of the six observations. For bins with less than 5 counts, we assign error bars as derived by Gehrels (1986), i.e., $1.0 + \sqrt{counts + 0.75}$; And for bins with greater than 5 counts we assign Poisson errors of $\sqrt{counts}$. The model with two PSFs yielded acceptable values of χ^2 in all the six cases. The best-fit χ^2 for each case is reported in the last column of Table 2. It should be noted that the effective exposure of all but observation ID 0206080101 are comparable. The observation length of 0206080101 is $\approx$ 100 ks while that of the rest of the observations is $\approx$ 25 ks. This dataset was also analyzed by Feng & Kaaret (2007) and they find that the long exposure causes the other dim sources nearby to be significant for surface brightness modeling. Therefore, to be consistent across all the observations we choose data from one of the good time intervals of MOS1 with effective exposure of 30 ks. This is comparable to the exposure times of the other four observations. The surface brightness contour maps of all of the six observations (centered on M82 X-1) are shown in Figure 1.

We estimated the individual average count rates of source 5 and M82 X-1 as follows. First, we estimated the total counts from a given source by integrating its best-fit PSF until the core radius. We then divide this by the total exposure time to calculate an average count rate. The formula for the count rate is therefore:

$$countrate = \frac{1}{T} \times \left(\int_{-r_0}^{+r_0} \frac{N}{\left[1 + \left(\frac{r}{r_0}\right)^2\right]^{\alpha}} 2\pi |r|\, dr \right)$$

where r is the radial distance from the centroid of the source and is defined as:

$$r = \sqrt{(x - x_0)^2 + (y - y_0)^2}$$

where (x_0, y_0) is the best-fit centroid position of a given source. N is the best-fit value of the normalization of a given source. T is the effective exposure time. The count rates of source 5 and M82 X-1 estimated with the method described above are shown in the second and the third columns of Table 2, respectively. In observation 0112290201, source 5 clearly dominates the overall X-ray flux from M82. However in the rest of the observations the flux from M82 X-1 is greater than the flux from source 5. Since the present work relies on the estimate of the spectral index of M82 X-1 with least possible contamination, we only considered observations in which the flux from M82 X-1 is $\gtrsim$ the flux from source 5. This filtering criterion resulted in a total of five observations (excluding observation 0112290201) to test for the timing-spectral correlation. We present the timing (PDS analysis) and the spectral analysis of these datasets in the following section.

3. Results

The following analysis (both timing and spectral) was carried out primarily using the EPIC-pn data with events in the energy range of 3.0-10.0 keV. We used the standard Science Analysis System (SAS) version 12.0.1 to reduce the light curves, the filtered event lists and the energy spectra. The standard filters of *(FLAG==0)* and *(PATTERN<=4)* were applied to all the datasets. The source events were extracted from a circular region of 33" centered around the brightest pixel in each observation. This particular radius value was chosen to include roughly 90% of the light from the source (as estimated from the fractional encircled energy of the EPIC-pn instrument). A background region of radius 50", free of other sources, was extracted from a nearby region. For a given observation, we used the same time intervals for extracting the power and the energy spectra. We also removed episodes of high background flaring from our analysis.

3.1. Timing Analysis

We constructed PDS from each of the five observations. These datasets, excluding observation 0206080101, have not been analyzed earlier and became public only recently (December 7^{th} 2012). The data from observation 0206080101 has already been analyzed by Mucciarelli et al. (2006) & Dewangan et al. (2006). We reanalyzed this observation to provide a consistent study of all the available data. All the PDS are shown in Figure 2 and Figure 3. The power spectra shown here use the so-called Leahy normalization, with the Poisson noise level being 2 (Leahy et al. 1983). It is clear that the overall behavior of all the PDS is the same. The power rises below $\approx$ 70-400 mHz with evidence for a QPO in the

range of ≈ 30-220 mHz; And essentially Poisson noise at higher frequencies. To quantify this behavior, we fit a power law to the continuum and a Lorentzian to model the QPO (Belloni et al. 2002). The mathematical representation of the model can be found within the index of Table 2. This model fits adequately in all the cases with reduced χ^2 in the range of 0.9-1.2. The best-fitting model parameters (derived from a fit in the frequency range of 0.001 Hz - 2.0 Hz) for each of the observation are shown in Table 3. We also indicate the χ^2/dof values for each of the fits along with the χ^2/dof corresponding to the continuum model (in braces). The change in the χ^2 serves as an indicator of the statistical significance of the QPOs.

The longest available EPIC-pn good time interval during the observation 0657801901 was only 8.8 ks. The significance (ftest) of the QPO detected in the PDS extracted from this short exposure was $\approx 3\sigma$. Fortunately, long uninterrupted data of duration ≈ 24 ks each was available from the MOS detectors. Therefore, to confirm the presence of the QPO, we extracted a PDS from the combined MOS data. The QPO is clearly evident in the MOS data with a detection significance of $\approx 5\sigma$. The 3-10 keV EPIC-pn and combined EPIC-MOS PDS are shown in the left and the right panels of Figure 3, respectively. It should be noted that we used the MOS data only in this instance, solely for the purpose of confirming the existence of the QPO. We did not use MOS data for any timing-spectral correlation studies. Finally, we analyzed the PDS of the backgrounds from each of the six datasets and note that they all are consistent with a constant Poisson noise.

As mentioned earlier, the source region of M82 X-1, used for extracting the PDS, is contaminated by nearby point sources. The major source of contamination is source 5 which can reach flux levels comparable to M82 X-1. Therefore it is a concern as to which source (M82 X-1 or source 5) produces the QPOs. Work by Feng & Kaaret (2007) has clearly shown that the few×10 mHz QPOs originate from M82 X-1. More specifically, they demonstrate that the 54 mHz QPO during the observation 0112290201 and the ≈ 120 mHz QPO during the observation 0206080101 originate from M82 X-1. Furthermore, Feng et al. (2008) used the high angular resolution observations by *Chandra* to extract a clean PDS of source 5. They find that in the frequency range of ≈ 30-220 mHz the PDS of source 5 is essentially noise (see Figure 1 of Feng et al. 2010), suggesting that the power spectral contamination by source 5 is negligible. It is therefore very likely that all the QPOs reported here (36-210 mHz) originate from M82 X-1. We discuss this issue further in the following section (See Figure 6).

3.2. Spectral Analysis

We used the SAS tool *evselect* to extract the source and the background spectra. The source spectra were then binned to one-third of the FWHM of the pn spectral resolution. We used the SAS task *specgroup* for this purpose. For each of the observation, the response files were generated using the *arfgen* and *rmfgen* tools that are part of the *XMM-Newton* SAS. The average 3-10 keV EPIC-pn count rate was in the range of $\approx$ 0.7-1.2 counts s^{-1}. Given such low count rates, source pileup was not an issue. We used the XSPEC (Arnaud 1996) spectral fitting package for modeling the X-ray spectra.

We fit all the energy spectra with a power-law (*powlaw* in XSPEC) and a Gaussian (*gauss* in XSPEC) modified by photoelectric absorption (*phabs* in XSPEC). The model was defined as *phabs*(powlaw+gauss)* in XSPEC. The hydrogen column density was set as a free parameter in all our fits. The gaussian component was used to model the weakly broadened iron line of M82 X-1 (Caballero-García 2011). Using high-quality data from *XMM-Newton* ($\approx$ 130 ks) and *Suzaku* ($\approx$ 100 ks), Caballero-García (2011) have demonstrated the presence of a weakly broadened Fe Kα emission line. They find that the best-fit values of the centroid energy and the width of the Fe Kα are independent of the continuum model and are in the range of 6.4-6.97 keV and 0.3-0.4 keV, respectively. The quality of our energy spectra does not allow us to constrain the properties of the iron line. However, they are required for a good-fit in every case. Therefore, we fixed the centroid energy and the width of the Gaussian component at 6.55 keV and 0.35 keV, respectively. These values are similar to those estimated by various authors including Strohmayer & Mushtozky (2003). This model gave acceptable fits in all the cases with reduced χ^2 in the range of 1.0-1.4. The best-fit model parameters of all the observations are shown in Table 3. A sample energy spectrum from observation 0657800101 is shown in Figure 4.

The effective exposure during the observation 0206080101 was $\approx$ 66 ks after accounting for the instrumental dead times and excluding good time intervals shorter than 5 ks. The three longest EPIC-pn good time intervals were of duration 33 ks, 20 ks and 13 ks. The PDS (see Table 2 and Section 3.1) of this observation was an average of six power spectra each of 10 ks duration. We split the light curve this way to maximize the available good time (signal to noise in the PDS $\propto \sqrt{exposuretime}$). To be consistent, we extracted energy spectra from the same time intervals, i.e., we extracted six energy spectra each of 10 ks duration. We then fit the model described above simultaneously to these six spectra. Therefore, we have a high total number of degrees of freedom compared to the other four energy spectra (see the last row of Table 3).

3.3. Timing-Spectral correlations

The primary goal of the present work is to understand the nature of the mHz QPOs from ULX M82 X-1 by testing for a timing-spectral correlation similar to that seen in StMBHs with type-C LFQPOs. The primary correlation that is characteristic of type-C LFQPOs in StMBHs is the dependence of the power-law index of the energy spectrum on the centroid frequency of the strongest QPO. Using all of the archival *XMM-Newton* observations we detected QPOs at five distinct frequencies from ULX M82 X-1 (see Section 3.1). We then extracted an energy spectrum in each of these cases and fit it with a power-law (see Section 3.2). Compiling all the results, we find that the power-law index of the energy spectrum shows an inverse dependence on the centroid frequency of the QPO. We find that as the centroid frequency of the QPO increases the power-law index of the energy spectrum tends to decrease. This is shown in the left panel of Figure 5. To estimate the significance of the correlation, we calculated the Pearson's correlation coefficient. We find that the value of the Pearson's correlation coefficient between the power-law index and the QPO frequency is -0.95.

In addition, we plot the resolved MOS1 X-ray (3-10 keV) count rate of M82 X-1 against the centroid frequency of the QPO. We find a stronger correlation with a Pearson's correlation coefficient of +0.97. We find that as the count rate of the source increases, the centroid frequency of the QPO also increases. This correlation is shown in the right panel of Figure 5.

4. Discussion

The so-called type-C LFQPOs of StMBHs are known to occur in the frequency range of $\sim$ 0.2-15 Hz. They are characterized by high quality factors (Q = centroid frequency/FWHM) of $\sim$ 7-12 and high fractional RMS amplitudes of $\sim$ 7-20% (see Table 1 of Casella et al. 2005, Table 2 of Remillard et al. 2002 and Table 1 of McClintock et al. 2009). Another distinct feature of the type-C LFQPOs of StMBHs is that their centroid frequency is tightly correlated with the power-law index of the X-ray energy spectrum (Sobczak et al. 2000a; Vignarca et al. 2003). The relationship can be described as an increase in the power-law index with the QPO frequency with evidence for turn-over at some higher value of the QPO frequency, i.e., beyond a certain high QPO frequency ($\sim$ 5-10 Hz) the power-law spectral index decreases with increasing QPO frequency. The turn-over is known to hold over a small range ($\sim$ 5-15 Hz) of QPO frequencies (See Figure 10 of Vignarca et al. 2003). This general behavior has now been observed from various StMBHs including XTE J1550-564 (Sobczak et al. 2000a; Vignarca et al. 2003; Shaposhnikov & Titarchuk 2009; McClintock et al. 2009),

GX 339-4 (Revnivtsev et al. 2001; Shaposhnikov & Titarchuk 2009; Stiele et al. 2013), GRO J1655-40 (Sobczak et al. 2000a; Vignarca et al. 2003; Shaposhnikov & Titarchuk 2009), Cygnus X-1 (Shaposhnikov & Titarchuk 2007, 2009), H1743-322 (Shaposhnikov & Titarchuk 2009; McClintock et al. 2009; Stiele et al. 2013), 4U 1543-475 (Shaposhnikov & Titarchuk 2009) and GRS 1915+105 (Vignarca et al. 2003; Titarchuk & Seifina 2009). While the slope of the correlation is different for different sources and sometimes different for the same source in a different outburst, the overall trend is the same.

It is interesting to note that the centroid frequency of the mHz QPOs of M82 X-1 appears to be **anti-correlated** with the power-law index of its energy spectrum over a wide range of QPO frequencies (36-210 mHz). There are two ways to interpret this result: (1) the mHz QPOs of M82 X-1 are indeed analogs of type-C LFQPOs of StMBHs with the observed anti-correlation representing the turn-over portion of the trend or (2) the mHz QPOs of M82 X-1 are fundamentally different from the type-C LFQPOs of StMBHs as they show distinctly inverse dependence on the power-law spectral index as opposed to the positive correlation seen in StMBHs. Assuming the former to be the case, one can estimate the mass of the black hole in M82 X-1 by simply scaling the turn-over frequency of M82 X-1 (anywhere in the range of $\approx$ 36-100 mHz) to the turn-over frequency observed in various StMBHs ($\approx$ 5-10 Hz). Under the assumption that the turn-over frequency scales inversely with the mass of the black hole, the mass of the black hole in M82 X-1 can be estimated to be in the range of $\approx$ 500-1000$M_{\odot}$, i.e., an IMBH. But on the other hand, an inverse dependence of power-law index on the QPO frequency has never been seen over such a wide range of QPO frequencies in StMBHs. In StMBHs such an inverse relationship is known to hold for QPO frequency changes of a factor of $\approx$ 1.5-3 (see Figure 10 of Vignarca et al. 2003; Shaposhnikov & Titarchuk 2009). The QPOs observed from M82 X-1 occur in the frequency range of 36-210 mHz. This represents a factor of $\approx$ 6 change in the centroid frequencies of the QPOs. Given such a large range in the QPO frequencies, it seems unlikley that the observed anti-correlation represents the turn-over portion of the type-C LFQPOs of StMBHs. In other words, the mHz QPOs of M82 X-1 may be fundamentally different compared to the type-C LFQPOs of StMBHs.

Furthermore, mHz QPOs in the range of $\approx$ 2-300 mHz (a frequency range comparable to QPOs of M82 X-1) have been observed from various StMBHs. These include GRO J0422+32 (QPOs with centroid frequencies of 300 mHz, 230 mHz and 200 mHz using Granat/SIGMA (40-150 keV), OSSE (35-60 keV) and BATSE (20-100 keV), respectively: Vikhlinin et al. 1995; Grove et al. 1998; van der Hooft et al. 1999), GRO J1719-24 (QPOs with centroid frequencies as low as 40 mHz and 300 mHz using BATSE (20-100 keV): van der Hooft et al. 1996), XTE J1118+480 (70-150 mHz QPOs detected using the USA experiment and RXTE: Wood et al. 2000; Revnivtsev et al. 2000), GX 339-4 (90-660 mHz QPOs using RXTE/PCA:

Revnivtsev et al. 2001), GRO J1655-40 (100 mHz QPO using RXTE/PCA: Remillard et al. 1999), XTE J1550-564 (80-300 mHz QPOs using RXTE/PCA: Remillard et al. 2002; Cui et al. 1999), GRS 1915+105 (2-160 mHz QPOs using RXTE/PCA: Morgan et al. 1997), Cygnus X-1 (40-70 mHz QPOs using Granat/SIGMA: Vikhlinin et al. 1994) and H1743-322 (11 mHz QPO using RXTE and *Chandra*: Altamirano & Strohmayer 2012). Moreover, the overall PDS of M82 X-1 shows similarities with the PDS of GRS 1915+105 when it exhibits a few×10 mHz QPOs and XTE J1550-564 when it shows a few×10 mHz QPOs (compare Figure 2 & 3 in this article with Figure 2 of Morgan et al. 1997 and Figure 2 of Cui et al. 1999). The continuum of the PDS of these three sources appear to be a simple power-law or a bending power-law. It is therefore possible that the mHz QPOs of M82 X-1 may be similar to the mHz QPOs of StMBHs; We are not able to observe the "higher-frequency" QPOs ($\sim$ 1-15 Hz) owing to very low count rate of M82 X-1 (Heil et al. 2009). If that were the case, the accreting black hole within M82 X-1 can be of stellar-mass. The large X-ray output may then be produced via some sort of a super-Eddington mechanism (see, for example, Begelman 2002).

On the other hand it is interesting to note that the X-ray intensity of the source correlates with the QPO centroid frequency. Such a dependence has been observed only from some StMBHs exhibiting type-C LFQPOs. These sources include XTE J1550-564 (see Figure 7 of Vignarca et al. 2003 and Table 1 of Sobczak et al. 2000b) and GRS 1915+105 (Figure 1 of Muno et al. 1999; Figure 1 of Reig et al. 2000; see Figure 2 & 3 of Rodriguez et al. 2002).

The observed anti-correlation hinges on the 210 mHz QPO (See the left panel of Figure 5). While it has been shown previously that M82 X-1 exhibits QPOs with centroid frequencies of $\approx$ 120 mHz and $\approx$ 50 mHz, a QPO with frequency as high as 210 mHz has never been reported from M82 X-1. To confirm that M82 X-1 is indeed the origin of this QPO, we carried out the same analysis as Feng & Kaaret (2007). We divided the source region into two semi-circles, one containing the majority of the flux from M82 X-1 (region A of the top panel of Figure 6) and the other dominated by the flux from source 5 (region B of the top panel of Figure 6). We then extracted the PDS from each of the individual half-circles. The PDS using only events from region A and from region B are shown in the middle and the bottom panel of Figure 6, respectively. It is clear that the QPO is evident in region A which is dominated by flux from M82 X-1. This analysis suggests that M82 X-1 is indeed the source of the 210 mHz QPO.

While the above analysis combined with earlier work by Feng & Kaaret (2007) demonstrates that the mHz QPOs in the frequency range of 36-210 mHz are likely from M82 X-1, there are other caveats concerning contamination from the nearby sources. We address some of them below:

(1) As discussed earlier, the *XMM-Newton* energy spectrum of M82 X-1 is contaminated by the flux from nearby point sources. While the other sources may be negligible, source 5 is known to reach flux levels greater than M82 X-1. By means of surface brightness modeling, we were able to exclude observations where source 5 was significantly more luminous than M82 X-1. However in the observations used for testing the correlation between the QPO centroid frequency and the power-law index, the flux from source 5 was not completely negligible. The count rate from source 5 during the observations 0206080101, 0657800101, 0657801901, 0657802101 and 0657802301 was 23%, 87%, 43%, 64% and 89% of the count rate of M82 X-1, respectively. It is not clear how this level of contamination can skew the value of the power-law index of the energy spectrum of M82 X-1. At present, *Chandra* is the only X-ray observatory that can resolve the individual point sources within M82 (e.g., Matsumoto et al. 2001, Jin et al. 2010). However, the effective area of *Chandra* is not sufficient to detect QPOs from M82 X-1. Therefore, to firmly establish the anti-correlation between the QPO centroid frequency and the power-law index, one would need simultaneous *Chandra* and *XMM-Newton* observations.

(2) The errorbars on the estimated power-law index are rather large. This makes it difficult to interpret the observed anti-correlation. Again *Chandra* data can solve this problem. M82 X-1 was observed with *Chandra/ACIS* (effective exposure of $\approx$ 50 ks) on 2005 February 4 (ObsID: 6097). Kaaret et al. (2006) have analyzed this observation and find that a simple power-law with a power-law index of 1.67 ± 0.02 adequately describes the data. As one can see the error on the power-law index is only $\approx 1.2\%$. Assuming the error value scales inversely with the $\sqrt{exposure}$, an exposure of roughly 10 ks with *Chandra* can give error values of $< 5\%$. Such errorbars will allow us to clearly judge the presence/absence of an anti-correlation.

(3) Another concern is regarding the specific spectral model to be used for the X-ray spectrum of M82 X-1. Recently, it has been suggested that ULXs may have inherently different X-ray energy spectra compared to StMBHs (Gladstone et al. 2009). More specifically, it has been argued that the X-ray energy spectra of ULXs may be better described by spectral models that allow for sharp rollovers above ≈ 5 keV. Spectral modeling of high-quality *XMM-Newton* , *Chandra* and *Suzaku/XIS* & *Suzaku/HXD* show some evidence for such a rollover in the energy spectrum of M82 X-1 (Agrawal & Misra 2006; Miyawaki et al. 2009). Nevertheless, it is currently not clear as to the exact model that describes the energy spectra of ULXs.

In summary, contamination from nearby point sources can in principle bias the value of the energy spectral power-law index and skew the dependence of the power-law index on the QPO frequency. An effective way to know for certain if the QPO centroid frequency of

ULX M82 X-1 is indeed anti-correlated with its power-law spectral index is through joint *Chandra/XMM-Newton* observations; Where the *Chandra* data can be used to extract clean energy spectra of M82 X-1 and the *XMM-Newton* data can be used to estimate the QPO parameters of the source.

REFERENCES

Agrawal, V. K., & Misra, R. 2006, ApJ, 638, L83

Altamirano, D., & Strohmayer, T. 2012, ApJ, 754, L23

Arnaud, K. A. 1996, Astronomical Data Analysis Software and Systems V, 101, 17

Begelman, M. C. 2002, ApJ, 568, L97

Belloni, T., Psaltis, D., & van der Klis, M. 2002, ApJ, 572, 392

Caballero-García, M. D. 2011, MNRAS, 418, 1973

Casella, P., Belloni, T., & Stella, L. 2005, ApJ, 629, 403

Chiang, Y.-K., & Kong, A. K. H. 2011, MNRAS, 414, 1329

Colbert, E. J. M., & Mushotzky, R. F. 1999, ApJ, 519, 89

Cui, W., Zhang, S. N., Chen, W., & Morgan, E. H. 1999, ApJ, 512, L43

Dewangan, G. C., Titarchuk, L., & Griffiths, R. E. 2006, ApJ, 637, L21

Dheeraj, P. R., & Strohmayer, T. E. 2012, ApJ, 753, 139

Feng, H., & Kaaret, P. 2007, ApJ, 668, 941

Feng, H., Rao, F., & Kaaret, P. 2010, ApJ, 710, L137

Fiorito, R., & Titarchuk, L. 2004, ApJ, 614, L113

Gehrels, N. 1986, ApJ, 303, 336

Gladstone, J. C., Roberts, T. P., & Done, C. 2009, MNRAS, 397, 1836

Grove, J. E., Strickman, M. S., Matz, S. M., et al. 1998, ApJ, 502, L45

Heil, L. M., Vaughan, S., & Roberts, T. P. 2009, MNRAS, 397, 1061

Immler, S., & Lewin, W. H. G. 2003, Supernovae and Gamma-Ray Bursters, 598, 91

Jin, J., Feng, H., & Kaaret, P. 2010, ApJ, 716, 181

Kaaret, P., Simet, M. G., & Lang, C. C. 2006, ApJ, 646, 174

King, A. R., Davies, M. B., Ward, M. J., Fabbiano, G., & Elvis, M. 2001, ApJ, 552, L109

Klein-Wolt, M., & van der Klis, M. 2008, ApJ, 675, 1407

Körding, E., Falcke, H., & Markoff, S. 2002, A&A, 382, L13

Körding, E. G., Migliari, S., Fender, R., et al. 2007, MNRAS, 380, 301

Leahy, D. A., Darbro, W., Elsner, R. F., et al. 1983, ApJ, 266, 160

Matsumoto, H., Tsuru, T. G., Koyama, K., et al. 2001, ApJ, 547, L25

McClintock, J. E., Remillard, R. A., Rupen, M. P., et al. 2009, ApJ, 698, 1398

McHardy, I. M., Koerding, E., Knigge, C., Uttley, P., & Fender, R. P. 2006, Nature, 444, 730

Miyawaki, R., Makishima, K., Yamada, S., et al. 2009, PASJ, 61, 263

Morgan, E. H., Remillard, R. A., & Greiner, J. 1997, ApJ, 482, 993

Mucciarelli, P., Casella, P., Belloni, T., Zampieri, L., & Ranalli, P. 2006, MNRAS, 365, 1123

Muno, M. P., Morgan, E. H., & Remillard, R. A. 1999, ApJ, 527, 321

Rao, F., Feng, H., & Kaaret, P. 2010, ApJ, 722, 620

Reig, P., Belloni, T., van der Klis, M., et al. 2000, ApJ, 541, 883

Remillard, R. A., Morgan, E. H., McClintock, J. E., Bailyn, C. D., & Orosz, J. A. 1999, ApJ, 522, 397

Remillard, R. A., Sobczak, G. J., Muno, M. P., & McClintock, J. E. 2002, ApJ, 564, 962

Revnivtsev, M., Sunyaev, R., & Borozdin, K. 2000, A&A, 361, L37

Revnivtsev, M., Gilfanov, M., & Churazov, E. 2001, A&A, 380, 520

Rodriguez, J., Durouchoux, P., Mirabel, I. F., et al. 2002, A&A, 386, 271

Shaposhnikov, N., & Titarchuk, L. 2007, ApJ, 663, 445

Shaposhnikov, N., & Titarchuk, L. 2009, ApJ, 699, 453

Sobczak, G. J., McClintock, J. E., Remillard, R. A., et al. 2000, ApJ, 531, 537

Sobczak, G. J., McClintock, J. E., Remillard, R. A., et al. 2000, ApJ, 544, 993

Stiele, H., Belloni, T. M., Kalemci, E., & Motta, S. 2013, MNRAS, 496

Strickland, D. K., & Heckman, T. M. 2007, ApJ, 658, 258

Strohmayer, T. E., Mushotzky, R. F., Winter, L., et al. 2007, ApJ, 660, 580

Strohmayer, T. E., & Mushotzky, R. F. 2003, ApJ, 586, L61

Strohmayer, T. E., & Mushotzky, R. F. 2009, ApJ, 703, 1386

Titarchuk, L., & Seifina, E. 2009, ApJ, 706, 1463

van der Hooft, F., Kouveliotou, C., van Paradijs, J., et al. 1996, ApJ, 458, L75

van der Hooft, F., Kouveliotou, C., van Paradijs, J., et al. 1999, ApJ, 513, 477

Vikhlinin, A., Churazov, E., Gilfanov, M., et al. 1994, ApJ, 424, 395

Vikhlinin, A., Churazov, E., Gilfanov, M., et al. 1995, ApJ, 441, 779

Vignarca, F., Migliari, S., Belloni, T., Psaltis, D., & van der Klis, M. 2003, A&A, 397, 729

Wijnands, R., & van der Klis, M. 1999, ApJ, 514, 939

Wood, K. S., Ray, P. S., Bandyopadhyay, R. M., et al. 2000, ApJ, 544, L45

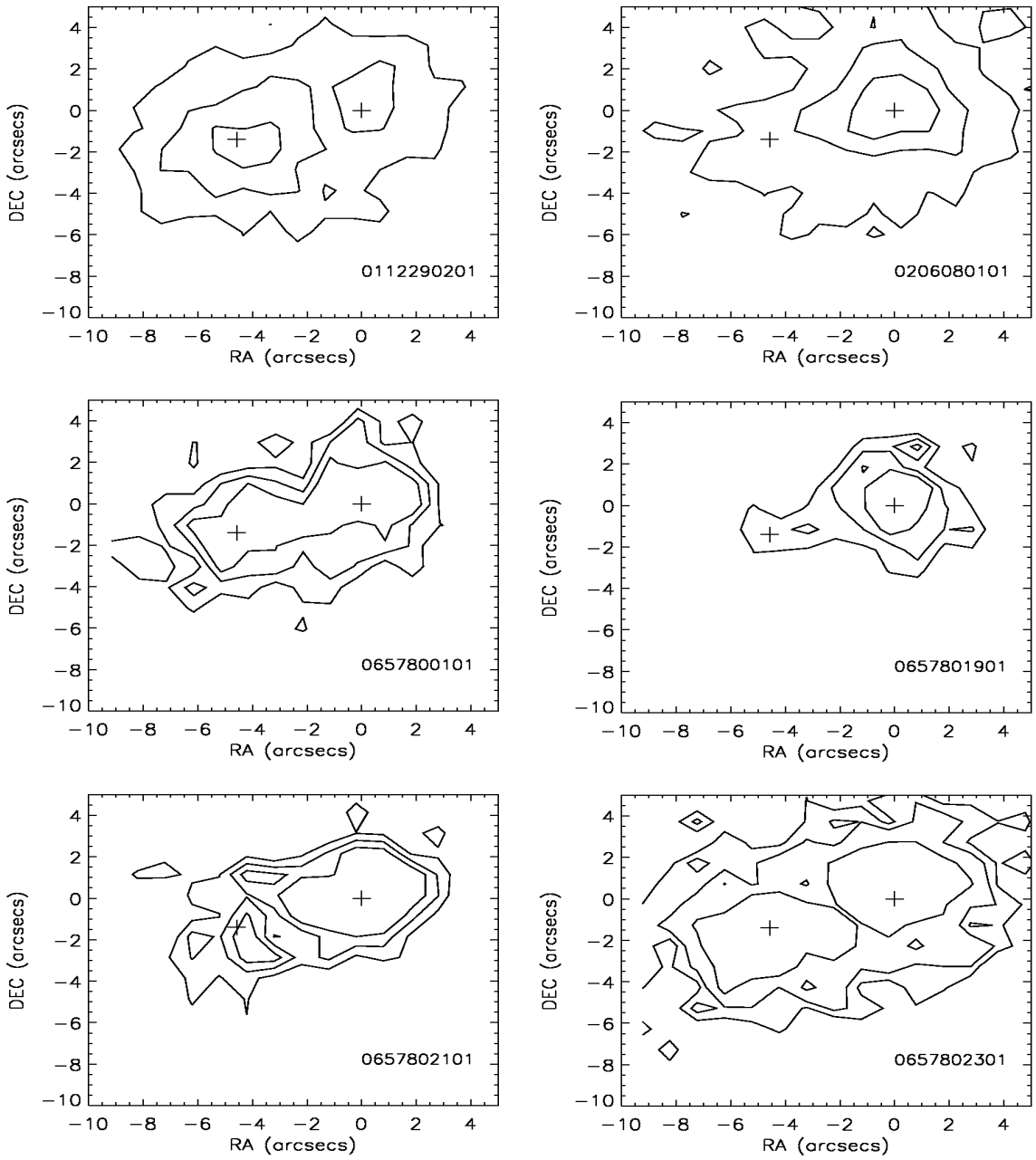

Figure 1: Surface brightness contour maps of the MOS1 images (3-10 keV) of M82 during six different epochs. The *XMM-Newton* assigned observation IDs are indicated at the bottom right of each panel. All the plots are centered on M82 X-1 and the best-fit positions of source 5 and M82 X-1 are represented by plus signs. Contour levels are different for different observations. Top left panel: The contour levels are 1.0, 1.75, 2.5 (10^{-3} counts s^{-1} $arcsec^{-2}$). Top right panel: The contour levels are 0.5, 1.0, 1.5 (10^{-3} counts s^{-1} $arcsec^{-2}$). Middle left panel: The contour levels are 0.75, 1.0, 1.25 (10^{-3} counts s^{-1} $arcsec^{-2}$). Middle right panel: The contour levels are 0.75, 1.0, 1.25 (10^{-3} counts s^{-1} $arcsec^{-2}$). Bottom left panel: The contour levels are 0.75, 1.0, 1.25 (10^{-3} counts s^{-1} $arcsec^{-2}$). Bottom right panel: The contour levels are 0.75, 1.0, 1.5 (10^{-3} counts s^{-1} $arcsec^{-2}$).

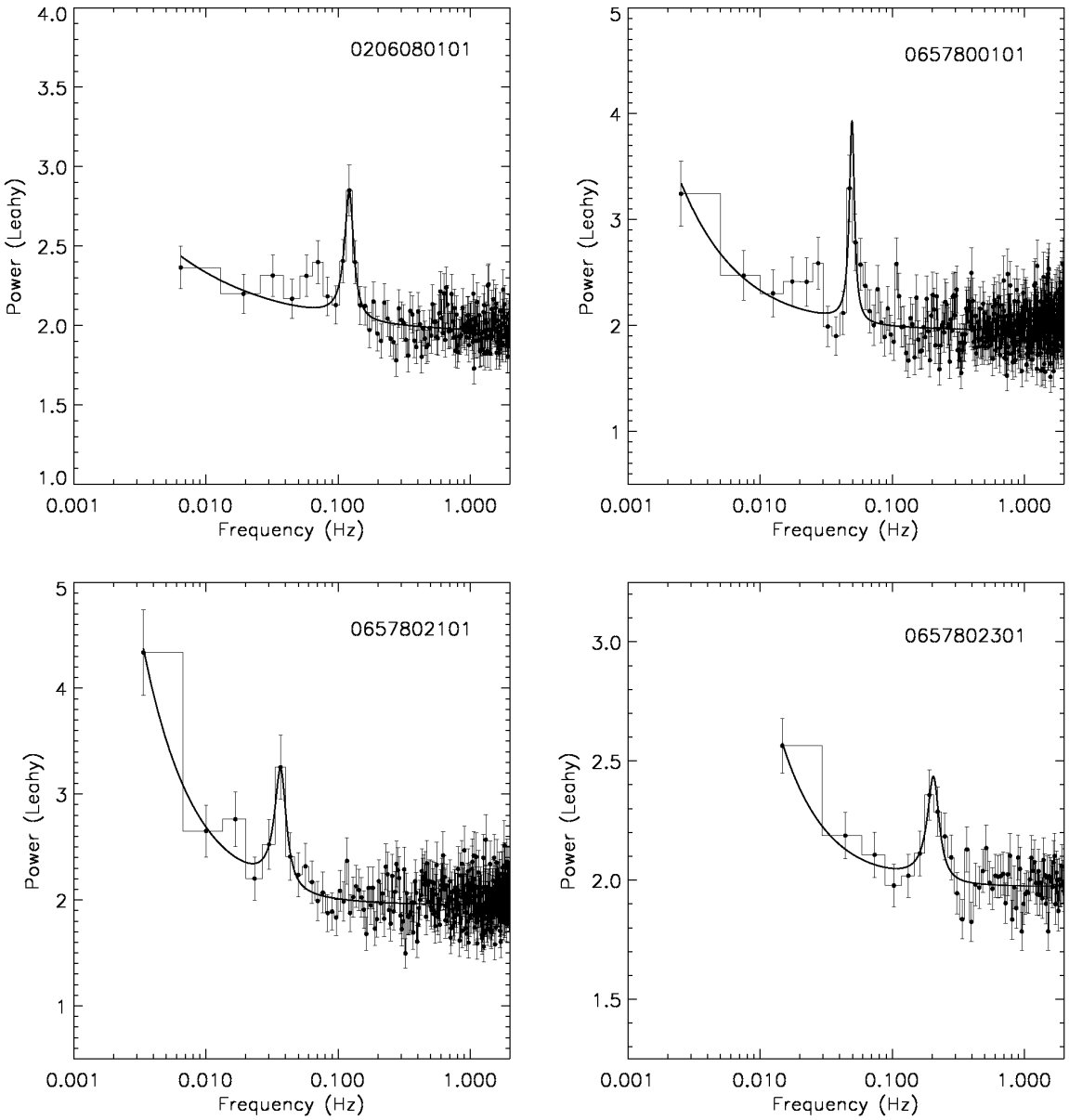

Figure 2: The EPIC-pn 3-10 keV power density spectra (*histogram*) and the best-fit model (*solid*) of four of the five *XMM-Newton* observations. The errorbars are also shown. The *XMM-Newton* assigned observation IDs are shown on the top right of each panel.

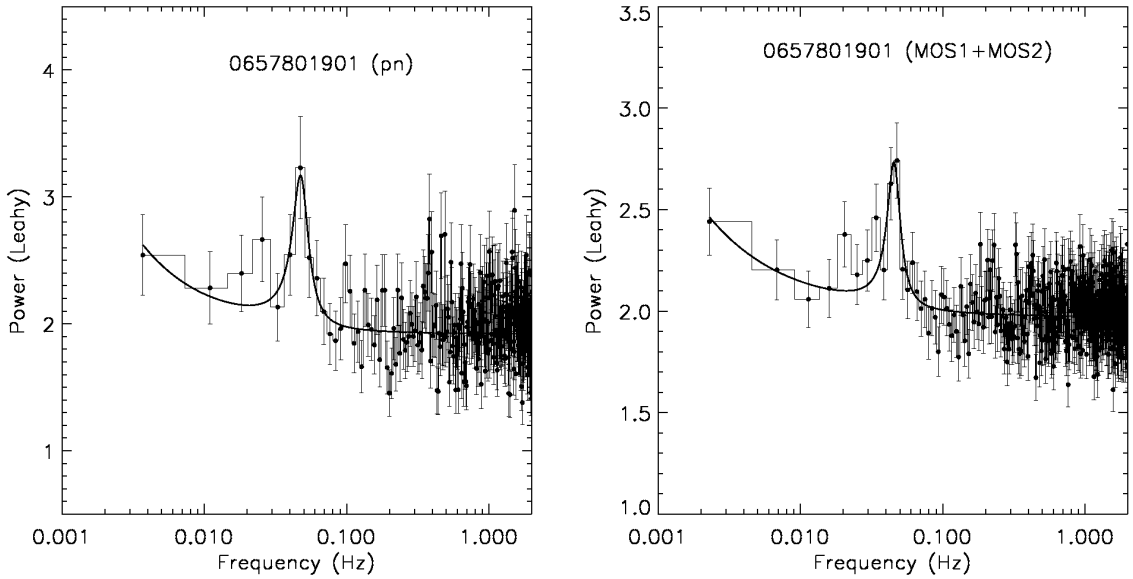

Figure 3: Left Panel: The EPIC-pn 3-10 keV power density spectrum (*histogram*) and the best-fit model (*solid*) of the observation ID 0657800101. Right Panel: The combined EPIC-MOS1 and EPIC-MOS2 3-10 keV power density spectrum (*histogram*) and the best-fit model (*solid*) of the same observation. In the EPIC-pn data the QPO is significant at only 3σ level. However, in the combined MOS power density spectrum the QPO is significant at 5σ level.

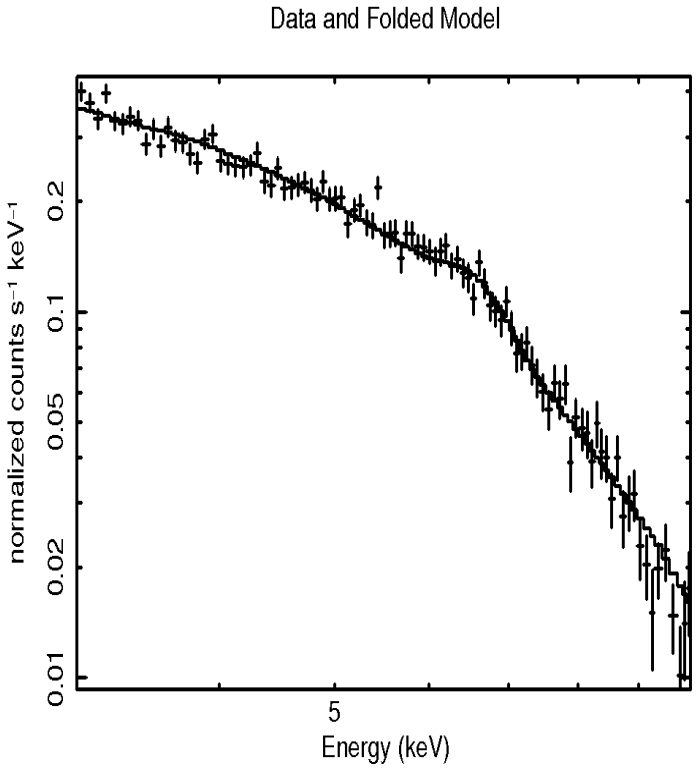

Figure 4: 3-10 keV EPIC-pn X-ray energy spectrum of M82 derived from observation 0657800101. The best-fit power-law + Gaussian (*phabs∗(powlaw+gauss)* in *XSPEC*) model is also shown (*solid*).

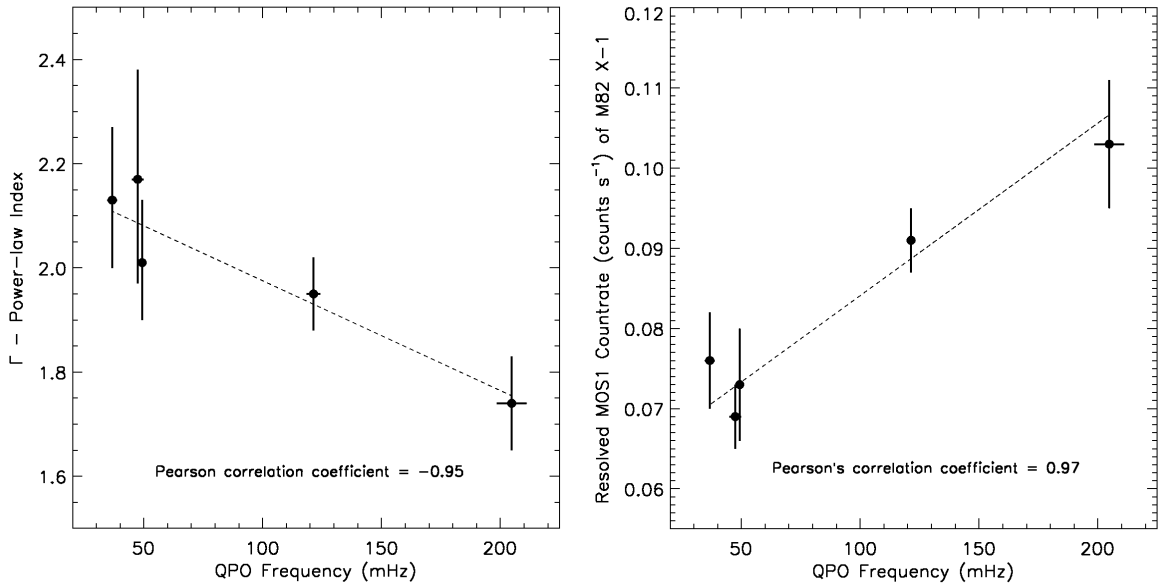

Figure 5: Timing-Spectral correlations. Left Panel: The dependence of the power-law index of the energy spectrum (*Y-axis*) on the centroid frequency of the QPO (*X-axis*). The errobars are also shown. Right Panel: The correlation between the resolved MOS1 count rate of M82 X-1 (*Y-axis*) is plotted against the centroid frequency of the QPO (*X-axis*). The errorbars are also shown. The value of the Pearson's correlation coefficient, which measures the significance of the correlation, is shown at the bottom of each panel. The best-fit straight lines (*dashed*) are also shown in each case.

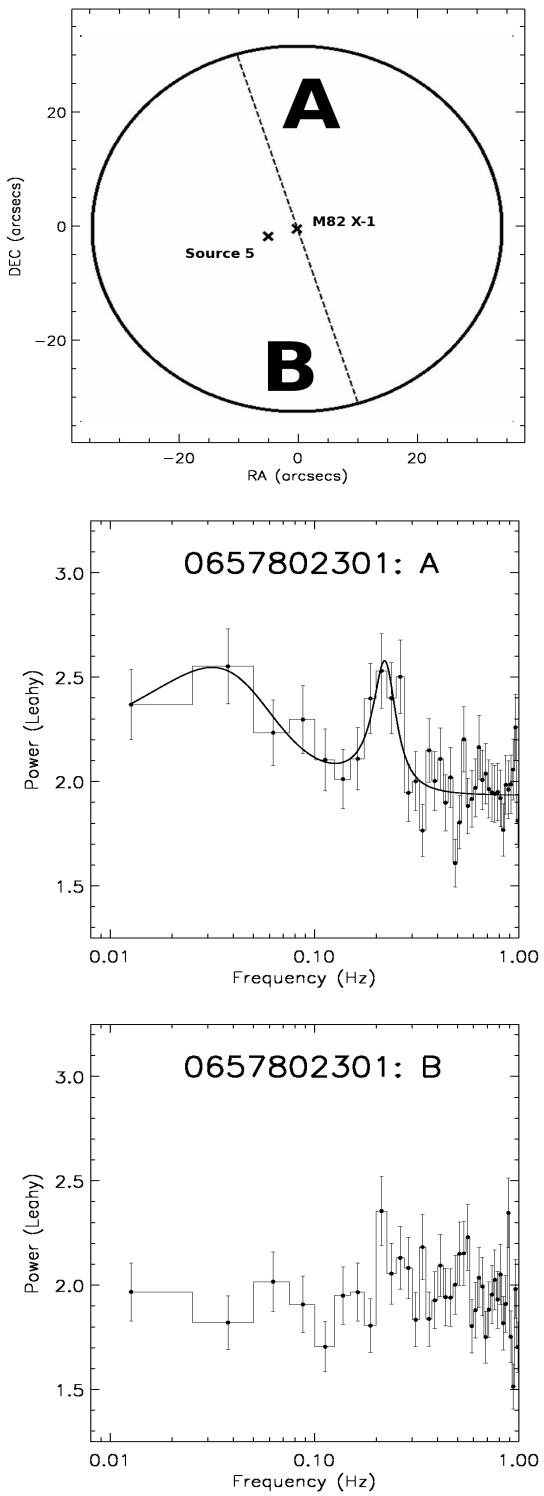

Figure 6: Top Panel: A circular source extraction region (radius of 33" and centered on M82 X-1) demarcated as region A (not containing source 5) and region B (containing source 5). Similar to Feng & Kaaret (2007), the dashed line is perpendicular to the line connecting M82 X-1 and source 5. Middle Panel: 3-10 keV EPIC-pn power density spectrum of region A. A best-fit model (bending power-law for the continuum and a Lorentzian for the QPO) is also shown (*solid*). Bottom Panel: 3-10 EPIC-pn power density spectrum of region B (*histogram*).

Table 1: Resolved average count rates (3-10 keV) of M82 X-1 and source 5 derived from the surface brightness modeling of *XMM-Newton*'s MOS1 images

ObsID[1]	Source 5 (counts s^{-1})[2]	M82 X-1 (counts s^{-1})[2]	χ^2/dof[3]
0112290201	0.141 ± 0.007	0.081 ± 0.007	627/437
0206080101	0.021 ± 0.003	0.091 ± 0.004	519/437
0657800101	0.068 ± 0.007	0.073 ± 0.007	420/437
0657801901	0.030 ± 0.004	0.069 ± 0.004	412/437
0657802101	0.049 ± 0.006	0.076 ± 0.006	440/437
0657802301	0.092 ± 0.008	0.103 ± 0.008	595/437

[1] The *XMM-Newton* assigned observation ID.

[2] The count rates are calculated using the formula described in the text (see Section 2).

[3] The χ^2/degrees of freedom (dof) was obtained by fitting two point spread functions to MOS1 images of size 21"×21" binned to 1"×1" and centered on M82 X-1.

Table 2: Summary of the 3-10 keV PDS modeling

ObsID	0206080101	0657800101	0657801901[c] (pn)	0657801901[c] (MOS)	0657802101	0657802301
Exposure[a] (ks)	60.0	22.0	8.8	24.2	17.4	17.0
A*	1.94 ± 0.04	1.96 ± 0.01	1.92 ± 0.02	1.97 ± 0.02	1.95 ± 0.01	1.97 ± 0.01
B*	0.03 ± 0.03	0.01 ± 0.01	0.01 ± 0.01	0.01 ± 0.01	0.01 ± 0.01	0.01 ± 0.01
Γ*	0.55 ± 0.23	1.09 ± 0.29	0.92 ± 0.64	0.76 ± 0.30	1.12 ± 0.22	1.28 ± 0.52
N_{QPO}†	0.81 ± 0.16	1.25 ± 0.29	1.19 ± 0.39	0.71 ± 0.18	1.13 ± 0.31	0.44 ± 0.18
ν_0† (mHz)	121.4 ± 2.9	49.3 ± 1.5	47.4 ± 2.5	45.4 ± 1.3	36.7 ± 2.1	204.8 ± 6.3
$\Delta\nu$† (mHz)	23.15 ± 6.22	8.6 ± 2.6	15.3 ± 6.8	12.0 ± 4.5	9.2 ± 3.6	51.8 ± 31.7
χ^2/dof (continuum[b])	137/150 (181/153)	381/338 (409/341)	310/269 (329/272)	442/434 (478/437))	317/294 (338/297)	53/62 (78/65)
Significance (ftest)	$> 5\sigma$	$\approx 3.9\sigma$	$\approx 3\sigma$	$\approx 5\sigma$	$> 3\sigma$	$\approx 3.9\sigma$

[a] The effective exposure used for extracting the power density spectra.

* We fit the continuum with a power-law model described as follows:

$$Continuum = A + B\nu^{-\Gamma}$$

where, Γ is the power-law index of the continuum.

† We model the QPOs with a Lorentzian. The functional form is as follows:

$$QPO = \frac{N_{QPO}}{1+\left(\frac{2(\nu-\nu_0)}{\Delta\nu}\right)^2}$$

where, ν_0 is the centroid frequency and $\Delta\nu$ is the FWHM of the QPO feature.

[b] The χ^2/dof for the continuum are shown in braces.

[c] Owing to only 8.8 ks of available good time interval, the significance of the QPO in the pn data was only 3σ. To confirm the presence of the QPO, we extracted a power density spectrum from combined MOS data. MOS data was used only for the purpose of confirming the QPO and was not used for timing-spectral correlation studies.

Table 3: Summary of the 3-10 keV energy spectral modeling. Our model was defined as *phabs∗(pow+gauss)* in *XSPEC*.

ObsID	0206080101	0657800101	0657801901	0657802101	0657802301
n_H[a]	$1.4^{+0.5}_{-0.5}$	$3.2^{+0.9}_{-0.9}$	$2.5^{+1.5}_{-1.5}$	$3.4^{+1.0}_{-1.0}$	$4.5^{+0.8}_{-0.8}$
Γ[b]	$1.95^{+0.07}_{-0.07}$	$2.01^{+0.12}_{-0.11}$	$2.17^{+0.21}_{-0.20}$	$2.13^{+0.14}_{-0.13}$	$1.74^{+0.09}_{-0.09}$
$N_{powerlaw}$[c]	$4.63^{+0.67}_{-0.58}$	$7.15^{+1.81}_{-1.42}$	$6.01^{+3.02}_{-1.96}$	$7.52^{+2.31}_{-1.73}$	$6.87^{+1.42}_{-1.16}$
N_{Fe}[d]	$2.50^{+0.44}_{-0.44}$	$2.68^{+0.95}_{-0.95}$	$3.18^{+1.15}_{-1.15}$	$3.28^{+0.96}_{-0.96}$	$4.27^{+1.25}_{-1.26}$
χ^2/dof	500/471[e]	102/95	90/66	98/92	132/95

[a] Total column density of hydrogen along the line of sight (in units of 10^{22} atoms cm^{-2}). We used the *phabs* model in XSPEC. [b] The photon index of the power law. [c] The normalization of the power-law component in units of 10^{-3}. [d] The normalization of the broad iron line in units of 10^{-5}. The centroid energy and the width of the broad iron line were fixed at the best-fit values found by Caballero-Garcí (2011). These values are 6.55 keV and 0.35 keV, respectively. [e] The power density spectrum extracted from this observation is an average of six good time intervals of 10 ks each. We use the same good time intervals for energy spectral analysis. This resulted in six energy spectra of 10 ks each. Hence, the higher number of degrees of freedom compared to other energy spectra where only one long good time interval was used.